SUPPORTING INFORMATION

Controlling Optoelectronic Properties of Carbazole-Pyridinium Luminophores via Kinetic Polymorphism

Roman Viter*[a], Matiss Martins Drava,[b] Alice Sciortino,[c] Mahmoud Abid,[d] Viktor Zabolotnii,[a] Marco Cannas,[c] Mikhael Bechelany,[d] and Artis Kinens*[b,e]

[a] *Institute of Atomic Physics and Spectroscopy, Faculty of Exact Sciences and Technologies, University of Latvia, Jelgavas street 3, Riga, LV 1004, Latvia. roman.viter@lu.lv*

[b] *Faculty of Medicine and Life Sciences, University of Latvia, Jelgavas street 1, Riga, LV 1004, Latvia. artis.kinens@lu.lv*

[c] *Physics and Chemistry Department - Emilio Segrè, University of Palermo, via archirafi 36, 90123, Palermo, Italy.*

[d] *Institut Européen des Membranes, IEM, UMR 5635, University of Montpellier, ENSCM, CNRS, Montpellier, France.*

[e] *Latvian Institute of Organic Synthesis, Aizkraukles street 21, LV-1006, Riga, Latvia*

Table of contents

Deconvolution of the photoluminescence spectrum 3

Grouping of Raman peaks 5

Lifetime and rates of radiative and non-radiative transitions 5

DFT calculations 6

Computational method 6

Geometries 8

Synthesis procedures of luminophore KL1421 9

General description 9

List of reagents and solvents 9

Synthesis procedures 10

^{1}H NMR spectra of synthesized compounds 13

References 16

Deconvolution of the photoluminescence spectrum

Deconvolution of the PL spectra has been performed by converting the measured absolute irradiance intensity from I(λ) to I(E) by applying the following equation λ:

$$I(E) = \frac{\lambda^2 \cdot I(\lambda)}{1240}$$

where λ is a wavelength in nm and E is a photon energy in eV.

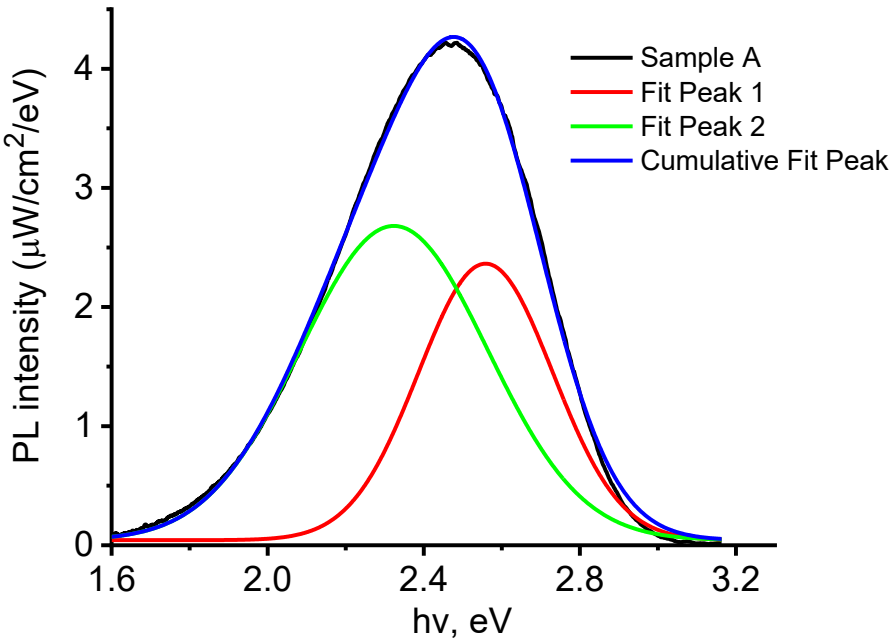

Figure S1. Deconvolution of the photoluminescence spectrum of polymorph A

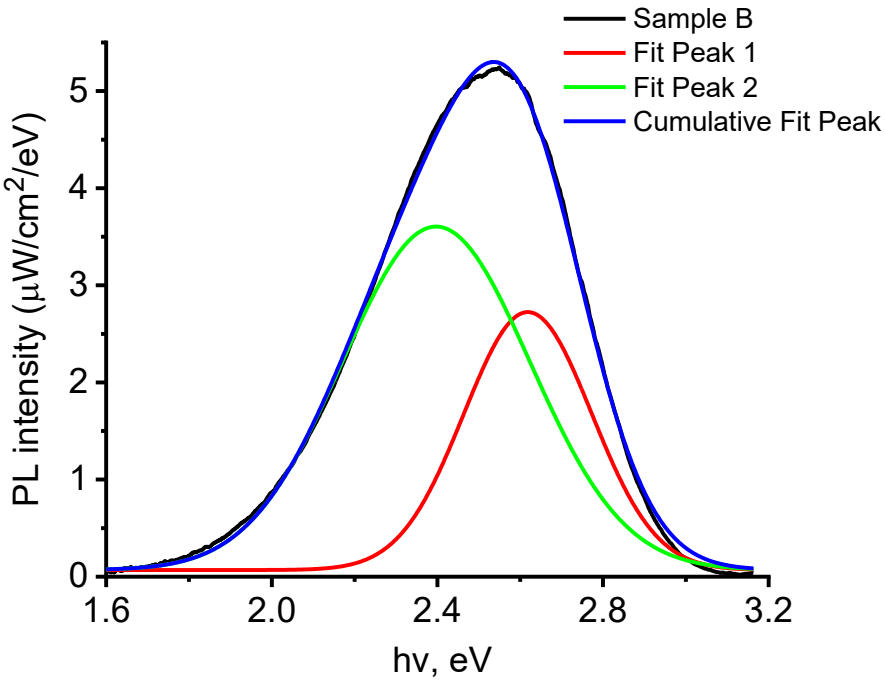

Figure S2. Deconvolution of the photoluminescence spectrum of polymorph B

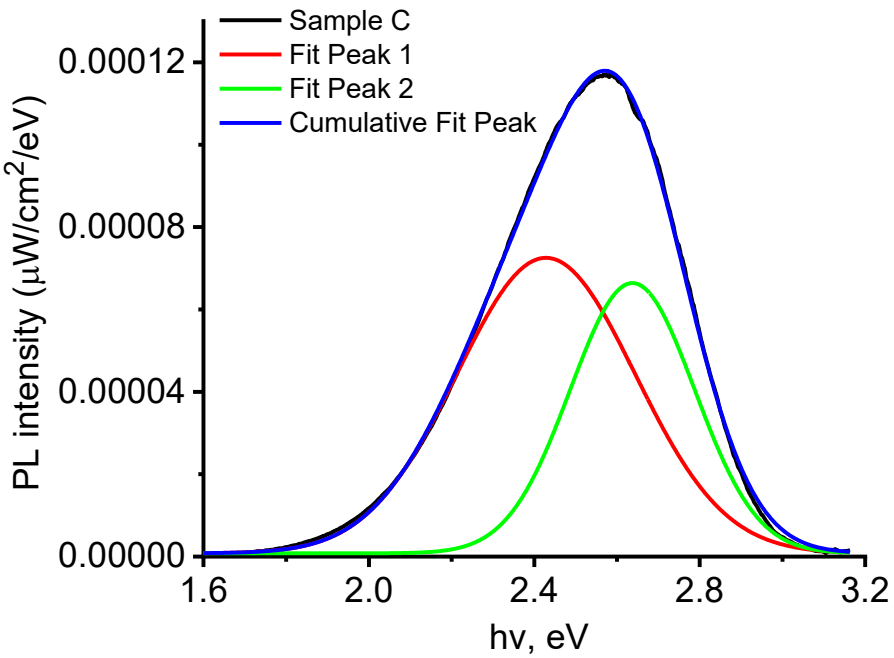

Figure S3. Deconvolution of the photoluminescence spectrum of polymorph C

Table S1. Deconvolution of PL spectra of polymorphs A-C

	Sample A		Sample B		Sample C	
Peak	2.56	2.32	2.62	2.4	2.57	2.33
FWHM	0.41	0.57	0.36	0.53	0.39	0.56
Height	2.32	2.64	2.66	3.54	2.34	2.89
area	1.00	1.59	1.03	2.01	0.98	1.72

Grouping of Raman peaks

Table S2

Raman peaks of polymorphs A-C

Sample A	Sample B	Sample C	Reference Raman[1–5]
97, 124, 158, 219, 335, 367, 426, 730, 775, 943, 959, 1022, 1043, 1125, 1213, 1246, 1296, 1302, 1323, 1369, 1440, 1456, 1477, 1566, 1582, 1601, 1631 cm^{-1}	110, 139, 171, 217, 234, 281, 308, 335, 364, 445, 477, 556, 732, 778, 943, 957, 1028, 1045, 1131, 1158, 1212, 1239, 1295, 1327, 1383, 1477, 1582, 1601, 1636 cm^{-1}	111, 136,170, 219, 310, 336, 367, 445, 474, 556, 648, 730, 779, 940, 959, 1029, 1045, 1130, 1158, 1212, 1239, 1296, 1321, 1338, 1386, 1474, 1581, 1602, 1632 cm^{-1}	946, 1081 cm^{-1} – S-O and S=O vibrations of the mesylate ion. 80-800 cm^{-1} – C-H rotation, bending, and deformation vibrations in the pyridinium ring; 800-1400 cm^{-1} – C-C, C-N, C-O, $-NH_2$ vibrations; 1400-1700 cm^{-1} – C=O, $-COO^-$, $-CH_3/CH_2$, C-C, C-N vibrations.

Lifetime and rates of radiative and non-radiative transitions

Table S3

Lifetime, quantum yields, and rates of radiative and non-radiative transitions in polymorphs

Sample	τ_1, ns	τ_2, ns	QY	k_r (ns^{-1})	k_{nr} (ns^{-1})
KL1421 A	60	250	0.61	0.006	0.004
KL 1421 B	142	-	0.8	0.006	0.0014
KL 1421 C	113	200	0.69	0.005	0.002

DFT calculations

Computational method

All calculations were performed using the Gaussian 09 software package.[6] Initial geometry optimization was performed without any restrictions using the B3LYP method and 6-31+g(d) basis set for all atoms. The obtained stationary point (Figure S4A, yellow-colored structure) was verified to be a real minimum (zero imaginary frequency) by performing frequency calculations at the same level of theory. The stationary point was used as a starting point for a potential energy scan using the same level of theory. The potential energy scan was obtained by incrementing the dihedral angle A-B-C-D (Figure S4A) by 5 ° until 180 ° rotation was achieved. The obtained potential energy surface revealed a second stationary point when the dihedral angle was increased by 50 ° (Figure S4B). The overlay of the initial stationary point (Yellow-colored structure) and the rotated geometry (Magenta-colored structure) is shown in Figure S4C. The energy of the second stationary point is 1.75 kcal/mol higher than that of the global minima. HOMO-LUMO energy gaps for both structures were obtained by single-point energy calculations using the B3LYP method and 6-31+g(d) basis set for all atoms. Finally, TD-DFT calculations at the same level of theory were performed to obtain energies of singlet and triplet excited states for both geometries (see Table S4).

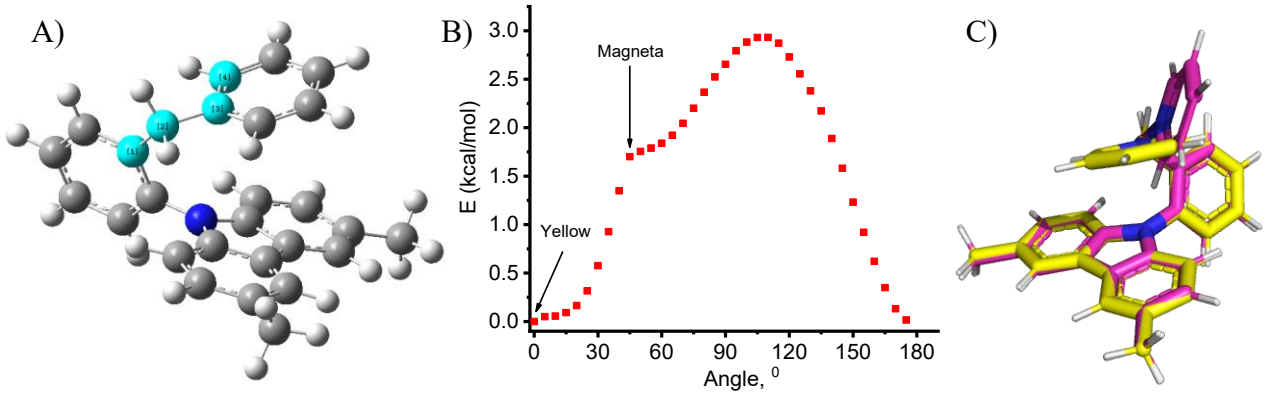

Figure S4. Dihedral angle used for potential energy scan (A), potential energy surface of pyridinium ring rotation relative to benzoyl subunit (B), and overlay of two energetic minima (C)

Table S4

Vertical excitation energies to singlet and triplet excited states

	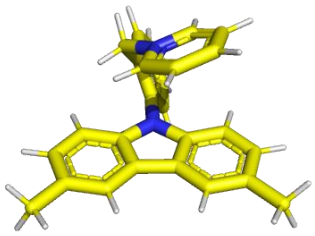			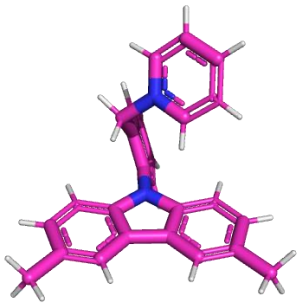		
State	**Singlet, eV**	**Triplet, eV**	**delta**	**Singlet, eV**	**Triplet, eV**	**delta**
1	1.7197	1.6170	-0.1027	1.3999	1.3956	-0.0043
2	1.9994	1.9864	-0.0130	1.7277	1.7235	-0.0042
3	2.5812	2.5586	-0.0226	2.3264	2.3217	-0.0047
4	2.9171	2.8956	-0.0215	2.6434	2.6273	-0.0161
5	2.9397	2.9037	-0.0360	2.6504	2.6436	-0.0068
6	3.5268	3.1253	-0.4015	3.3640	3.1028	-0.2612
7	3.6250	3.2840	-0.3410	3.4265	3.2255	-0.2010
8	3.7538	3.3320	-0.4218	3.5032	3.3178	-0.1854
9	3.8016	3.5749	-0.2267	3.5482	3.3834	-0.1648
10	3.8399	3.6802	-0.1597	3.5603	3.4600	-0.1003
11	3.8833	3.6990	-0.1843	3.7205	3.4931	-0.2274
12	3.9283	3.7274	-0.2009	3.7505	3.5384	-0.2121
13	3.9489	3.7922	-0.1567	3.9545	3.5476	-0.4069
14	4.3003	3.8737	-0.4266	4.1020	3.7234	-0.3786
15	4.4174	3.9072	-0.5102	4.3627	3.8297	-0.5330
16	4.5788	3.9121	-0.6667	4.4246	3.9191	-0.5055

Geometries

Yellow

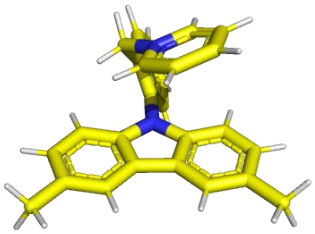

E(RB3LYP) = -1113.97147813 (Hartree/Particle)

1 1

C	-2.23468900	-2.79442900	-1.32087800
C	-0.86035400	-3.04545800	-1.53753000
C	0.11053400	-2.05223800	-1.41096600
C	-0.31594000	-0.76800700	-1.05919300
C	-1.68360300	-0.48270300	-0.82726000
C	-2.63456800	-1.50450000	-0.96048600
H	-0.54936100	-4.04651200	-1.82830600
H	1.15657600	-2.27270000	-1.60450200
H	-3.68888500	-1.29206800	-0.79711600
C	-0.44855100	1.43948700	-0.52743900
C	-0.18721800	2.79391200	-0.29203700
C	-1.26906700	3.62129100	0.00992500
C	-2.59693300	3.13912600	0.07311400
C	-2.83425400	1.78546200	-0.18162800
C	-1.76846500	0.92561200	-0.48584300
H	0.81608400	3.20365000	-0.37768600
H	-1.08562500	4.67895200	0.18483400
H	-3.85245300	1.40333500	-0.15991100
C	1.85042900	0.50063500	-0.95956700
C	2.46346100	0.34070900	-2.20614000
C	2.64067500	0.73394800	0.18786100
C	3.85262600	0.42398200	-2.32755300
H	1.84031900	0.16628300	-3.07832500
C	4.03167600	0.82859800	0.04695000
C	4.63884900	0.67601300	-1.20177100
H	4.31587900	0.30504800	-3.30271300
H	4.64713500	1.02491500	0.92222800
H	5.71830700	0.75234200	-1.29140200
C	2.01980700	0.92042400	1.55202300
H	1.34642000	1.77946000	1.58186800
H	2.79715400	1.07220000	2.30621100
C	-0.05762200	-0.05506500	2.47649300
C	1.74187000	-1.49510700	1.99194400
C	-0.81229700	-1.11700000	2.95150800
H	-0.43035100	0.96144300	2.44466100
C	1.03189900	-2.58643200	2.46121800
H	2.74583700	-1.56943600	1.59076800
C	-0.26466500	-2.40034200	2.95034100
H	-1.81793300	-0.92789200	3.31023800
H	1.49388300	-3.56729400	2.43787200
H	-0.83916700	-3.24439600	3.31921200
N	1.19719600	-0.25409200	2.00928700
N	0.43618200	0.40006100	-0.85055500
C	-3.73360500	4.08936700	0.37643600
H	-4.68007200	3.55371200	0.49969600
H	-3.54821000	4.65984200	1.29454800
H	-3.86840200	4.81730100	-0.43362800
C	-3.24793400	-3.90047700	-1.51519500
H	-4.23307000	-3.61184400	-1.13506300
H	-3.36469800	-4.14770400	-2.57820500
H	-2.94537800	-4.82128000	-1.00237900

Magenta

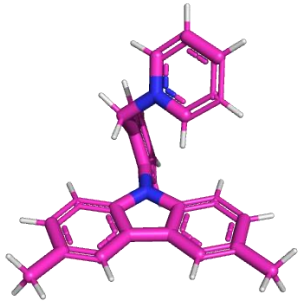

E(RB3LYP) = -1113.96868176 (Hartree/Particle)

1 1

C	-2.17102800	3.35075500	0.73524600
C	-0.92918400	3.22235100	1.39790900
C	-0.24947600	2.00658900	1.48333300
C	-0.84132500	0.88785900	0.88735600
C	-2.08350000	0.98095100	0.21361800
C	-2.73749300	2.21945100	0.14171300
H	-0.49241800	4.09970600	1.87009300
H	0.69498500	1.93664700	2.01621500
H	-3.69414600	2.30003700	-0.36930900
C	-1.33958400	-1.19723800	0.11804400
C	-1.36061000	-2.56746100	-0.15810300
C	-2.45809900	-3.07020900	-0.85674000
C	-3.52750400	-2.24876200	-1.27994700
C	-3.48898600	-0.88520800	-0.97836700
C	-2.40138900	-0.34847200	-0.27472000
H	-0.56989800	-3.23109500	0.18222000
H	-2.49677300	-4.13558700	-1.07246100
H	-4.31189700	-0.24182600	-1.28088300
C	0.79978400	-0.94148000	1.42611200
C	0.86620500	-0.97197800	2.82444200
C	1.89035300	-1.41311700	0.66373500
C	2.00139800	-1.46257200	3.47063700
H	0.01363200	-0.61767700	3.39619400
C	3.01125600	-1.93028100	1.32945000
C	3.07597400	-1.95062500	2.72259200
H	2.03716300	-1.48272400	4.55604000
H	3.84274900	-2.32941600	0.75172900
H	3.95277500	-2.35478700	3.21957500
C	1.87118500	-1.38722700	-0.84927100
H	0.85800400	-1.42086100	-1.25103700
H	2.42731000	-2.23138800	-1.26103000
C	1.82723800	1.01898600	-1.41989300
C	3.76677000	-0.21198500	-1.93716000
C	2.39483200	2.17517000	-1.93311400
H	0.83353700	0.99280600	-0.98811000
C	4.37894500	0.91484900	-2.46190800
H	4.24921200	-1.18183300	-1.91375700
C	3.68652300	2.12884300	-2.46180800
H	1.81875000	3.09385000	-1.91421300
H	5.38200000	0.83261700	-2.86618900
H	4.14666400	3.02331200	-2.87063700
N	2.51448600	-0.14835300	-1.42584700
N	-0.36727500	-0.43314900	0.79073800
C	-4.69555400	-2.85238500	-2.02720800
H	-5.42381100	-2.08733300	-2.31397200
H	-4.36694500	-3.36064300	-2.94213700
H	-5.21910200	-3.59660300	-1.41418200
C	-2.87516300	4.68886200	0.69710600
H	-3.76200900	4.65474300	0.05661800
H	-3.20210700	4.99420100	1.69922500
H	-2.21756800	5.48038900	0.31745200

Synthesis procedures of luminophore KL1421

General description

The solvents and reagents used were purchased from commercial sources, including Acros Organics, Sigma-Aldrich, Alfa Aesar, Fisher Chemical, and Fluorochem, and were used without further purification. The reaction progress was monitored using an LC-MS system consisting of an Agilent InfinityLab LC 1290 MSD system with an Agilent InfinityLab Poroshell 120 EC-C18 3.0 x 50 mm, 2.7 µm LC column, and a 0.5 $mL \cdot min^{-1}$ flow rate. The gradient eluent from 90:10 of 0.01% TFA aqueous solution/MeCN to 5:95 of 0.01% TFA aqueous solution/MeCN was used for analysis.

The obtained compound's ^{1}H NMR spectra were recorded in $CDCl_3$ and MeOD-*d*$_4$ solutions using a Bruker Fourier-300 spectrometer. For the ^{1}H NMR spectrum, the non-deuterated residual signals of $CDCl_3$ (7.26 ppm) and MeOD-*d*$_4$ (3.31 ppm) were used as internal standards. Chemical shifts are reported in the δ scale, and *J* constants were measured in hertz (Hz). Multiplicities are indicated with the symbols: s (singlet), d (doublet), t (triplet), q (quartet), and m (multiplet).

List of reagents and solvents

Reagents used for synthesis:

3,6-Dimethyl-9*H*-carbazole (*BLDpharm*, purity: 95%, CAS: 5599-50-8), Ethyl 2-bromobenzoate (*Fluorochem*, purity: 99%, CAS: 6091-64-1), Potassium carbonate (**K_2CO_3**) (*Fischer scientific*, purity: ≥99.5 %, CAS: 584-08-7), *L*-Proline (*Fluorochem*, purity: ≥99%, CAS: 147-85-3), Copper (I) iodide (**CuI**) (*Alfa Aesar*, purity: ≥99%, CAS: 7681-65-4), Lithium aluminium hydride (**$LiAlH_4$**), 4.0 M in diethyl ether (*Acros organics*, purity: ≥99%, CAS: 16853-85-3) Methanesulfonyl chloride (**MsCl**) (*Sigma-Aldrich*, purity: ≥99.7%, CAS: 124-63-0), *N,N*-Diisopropylethylamine (**DIPEA**) (*Tokyo chemical industry* (*TCI*), purity: 99%, CAS: 7087-68-5), Pyridine (**Py**) (*Acros organics*, purity: 99.5%, CAS: 110-86-1).

Solvents used for synthesis and purification:

Anhydrous dimethylsulfoxide (**DMSO**) (*Acros organics*, purity: ≥99.7%, CAS: 67-68-5), Ethyl acetate (**EtOAc**) (*Fischer scientific*, purity: 99.8 %, CAS: 141-78-6), Petrolium ether (**PE**) (40-60°C) (*Fischer scientific*, CAS: 8032-32-4), Anhydrous tetrahydrofuran (**THF**) (*Acros organics*, purity: ≥99%, CAS: 109-99-9), Dichloromethane (**DCM**) (*Fischer scientific*, purity: 99.8 %, CAS: 75-09-2), Acetonitrile (**MeCN**) (*Fischer scientific*, purity: 99.9 %, CAS: 75-05-8), Diethyl ether (**Et_2O**) (*Fischer scientific*, purity: ≥99 %, CAS: 60-29-7), Methyl-tert-butyl ether (**MTBE**) (*Fischer scientific*, purity: ≥99.5 %, CAS: 1634-04-4).

Deuterated solvents for product characterization:

Deuterated chloroform (**$CDCl_3$**) (*Eurisotop*, CAS: 865-49-6), Deuterated methanol (**MeOD-*d_4***) (*Eurisotop*, CAS: 811-98-3)

Synthesis procedures

Synthesis of luminophore KL1421 was performed by following the experimental procedure reported by Leduskrasts et al. (see Figure S5).[7] First, aryl carbazole derivative **3** was obtained in 85% yield in the Ullmann coupling from commercially available carbazole **1** and benzoic acid derivative **2**. Then ester **3** was reduced using $LiAlH_4$, yielding benzyl alcohol **4** in 98% yield. Finally, subsequent mesylation and nucleophilic substitution yielded the target compound KL1421 in 70% yield over two steps.

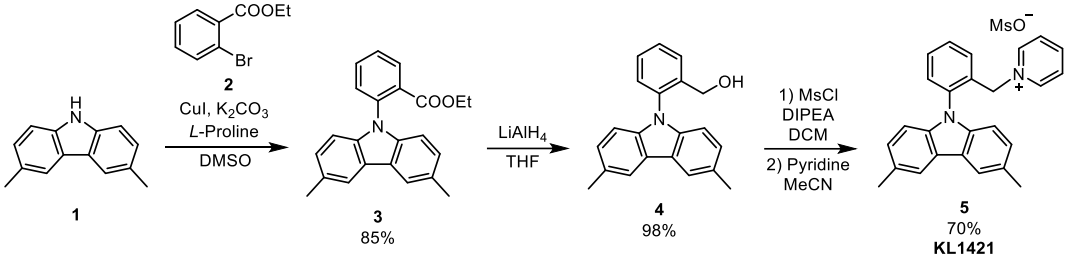

Figure S5. Synthesis scheme of luminophore KL1421[7]

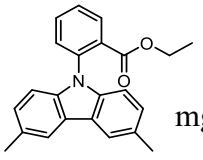

Ethyl 2-(3,6-dimethyl-9*H*-carbazol-9-yl)benzoate (**3**). Carbazole **1** (0.40 g, 2.00 mmol, 1.0 equiv.), K_2CO_3 (1.00 g, 7,70 mmol, 3.9 equiv.) and *L*-proline (88.0 mg, 0.80 mmol, 0.4 equiv.) were loaded in a 25 mL pressure vial. The vial was dried under vacuum for 10 min at 60 °C. Then CuI (120 mg, 0.60 mmol, 0.3 equiv.) was added, and the vial was purged with argon and sealed. Then ethyl 2-bromobenzoate (**2**) (0.80 ml, 5.00 mmol, 2.5 equiv.) was added, followed by anhydrous DMSO (9 mL). The argon was bubbled through the blue suspension for 10 min and then heated at 145 °C for 48 h. After cooling, the brown suspension was diluted with water (50 mL) and extracted with DCM (4×70 mL). The combined organic layers were dried over anhydrous Na_2SO_4 and purified by *flash* column chromatography (SNAP 60 g C18 column, 40 mL/min flow rate, gradient from 75% H_2O to 100% MeCN, over 12 CV). Fractions containing product **3** were combined and purified by *flash* column chromatography (100 g SiO_2 column, 30 mL/min flow rate, from 2% EtOAc to 91% petroleum ether) to obtain **3** as a colorless viscous oil (0.57 g, 85 %); analytical TLC on silica gel, 1:10 EtOAc/petroleum ether, R_f =0.40.

^{1}H NMR (300 MHz, $CDCl_3$) δ 8.14 – 8.06 (m, 1H), 7.90 – 7.85 (m, 2H), 7.76 – 7.69 (m, 1H), 7.61 – 7.52 (m, 2H), 7.20 – 7.13 (m, 2H), 7.03 – 6.97 (m, 2H), 3.68 (q, *J* = 7.1 Hz, 2H), 2.53 (s, 6H),

0.44 (t, J = 7.1 Hz, 3H). The ^{1}H-NMR spectrum of the obtained compound corresponds to that reported in the literature.[7]

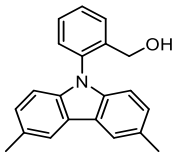

(2-(3,6-Dimethyl-9*H*-carbazol-9-yl)phenyl)methanol (**4**). Anhydrous THF (10 mL) solution of ethyl 2-(3,6-dimethyl-9H-carbazol-9-yl)benzoate (**3**) (0.54 g, 1.60 mmol, 1.0 equiv.) was dropwise added to a $LiAlH_4$ solution (4M, 1.00 mL, 4.00 mmol, 2.5 equiv) in diethyl ether at 0 °C. The white suspension was stirred at room temperature for 1 h. Then cooled in an ice bath and quenched in a sequence by dropwise addition of water (0.15 mL), aqueous 4M NaOH solution (0.30 mL), and water (0.45 mL). The obtained white suspension was filtered through a pad of Celite, washed with THF, and evaporated to yield product **4** as a viscous colorless oil (0.47 g, 98 %).

^{1}H NMR (300 MHz, $CDCl_3$) δ 7.96 – 7.88 (m, 2H), 7.81 – 7.73 (m, 1H), 7.62 – 7.46 (m, 2H), 7.40 – 7.32 (m, 1H), 7.23 – 7.15 (m, 2H), 6.97 – 6.85 (m, 2H), 4.33 (s, 2H), 2.55 (s, 6H). The ^{1}H-NMR spectrum of the obtained compound corresponds to that reported in the literature.[7]

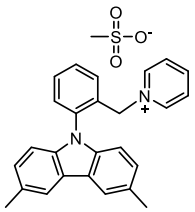

1-(2-(3,6-Dimethyl-9*H*-carbazol-9-yl)benzyl)pyridin-1-ium methanesulfonate (**5**) **KL1421**. (2-(3,6-Dimethyl-9H-carbazol-9-yl)phenyl)methanol (**4**) (0.15 g, 0.50 mmol, 1.0 equiv) was dissolved in anhydrous DCM (7.6 mL), and the solution was cooled to 0 °C. MsCl (77.0 µL, 1.00 mmol, 2.0 equiv.) and DIPEA (0.40 mL, 2.00 mmol, 4.0 equiv.) were added to the solution, and the obtained pale yellow solution was stirred at 0 °C for 1 h. Then the reaction mixture was diluted with DCM (13 mL) and water (13 mL), the layers were separated, and the organic layer was extracted with water (20 mL). The organic layer was dried over anhydrous Na_2SO_4 and concentrated under reduced pressure. The residue was dissolved in MeCN (2.5 mL) to give a clear, yellow solution. Pyridine (0.40 mL, 5.00 mmol, 10.0 equiv.) was added to the solution. The solution was stirred at room temperature. After 72 h, the reaction mixture was diluted with Et_2O (50 mL), and the white suspension was filtered under an argon atmosphere. The precipitates were dissolved in MeCN (20.0 mL), and activated charcoal was added to the yellow solution. The black suspension was heated at 50 °C for 10 min, filtered through a celite pad, and evaporated under reduced pressure to ~ 2 mL. Then Et_2O (50 mL) was added to the yellow solution, and the white suspension was filtered under an argon atmosphere. The precipitates (162 mg, 70 %) were washed with Et_2O and recrystallized to yield three distinct polymorphs.

^{1}H NMR (300 MHz, MeOD-d4) δ 8.04 – 7.93 (m, 2H), 7.93 – 7.86 (m, 2H), 7.87 – 7.73 (m, 4H), 7.62 – 7.46 (m, 1H), 7.43 – 7.28 (m, 2H), 7.19 – 7.06 (m, 2H), 6.73 – 6.63 (m, 2H), 5.56 (s, 2H),

2.68 (s, 3H), 2.51 (s, 6H). The ^{1}H-NMR spectrum of the obtained compound corresponds to that reported in the literature.[7]

^{1}H NMR spectra of synthesized compounds

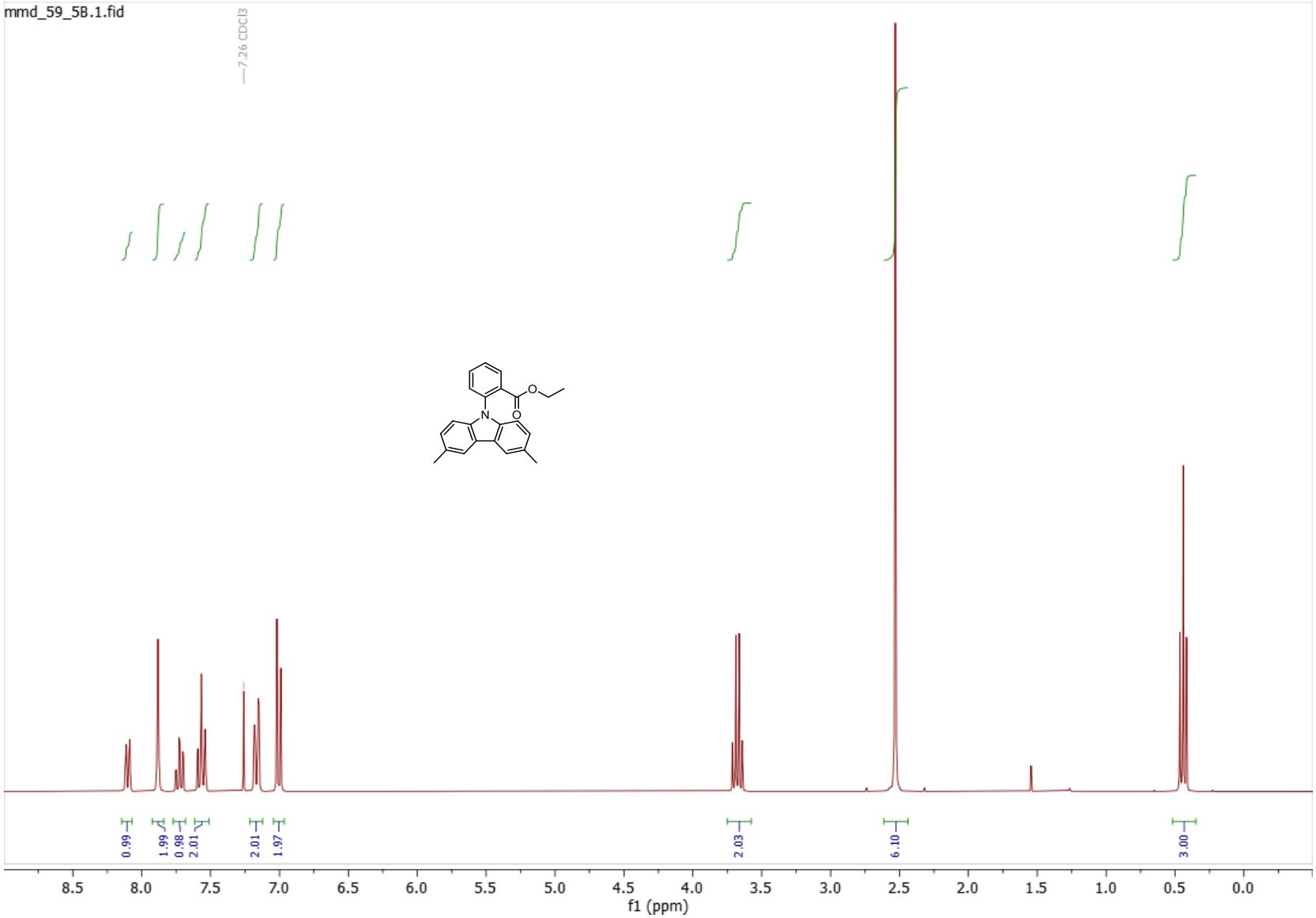

Figure S6. ^{1}H NMR of ethyl 2-(3,6-dimethyl-9*H*-carbazol-9-yl)benzoate (**3**)

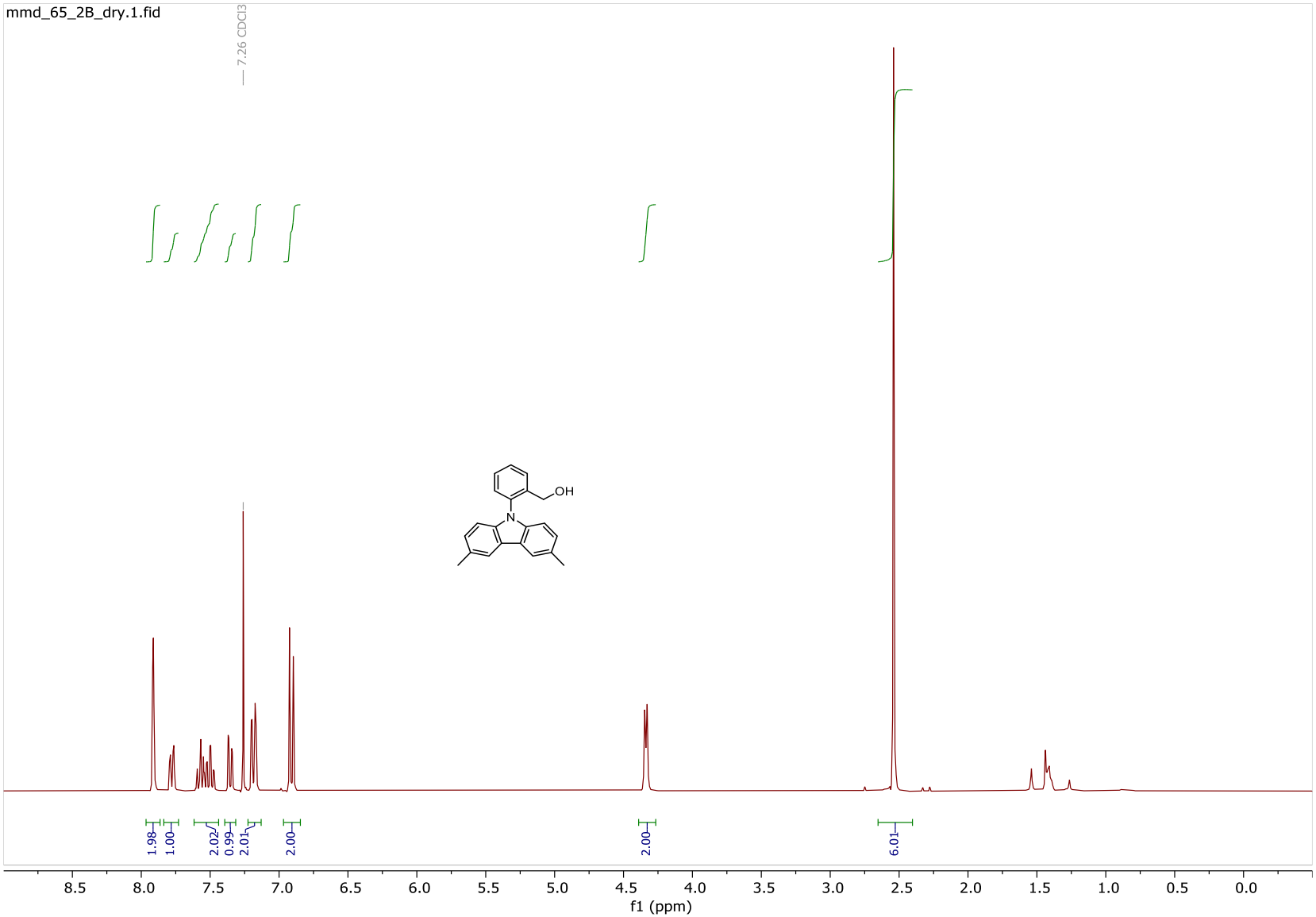

Figure S7. ^{1}H NMR of (2-(3,6-dimethyl-9*H*-carbazol-9-yl)phenyl)methanol (**4**)

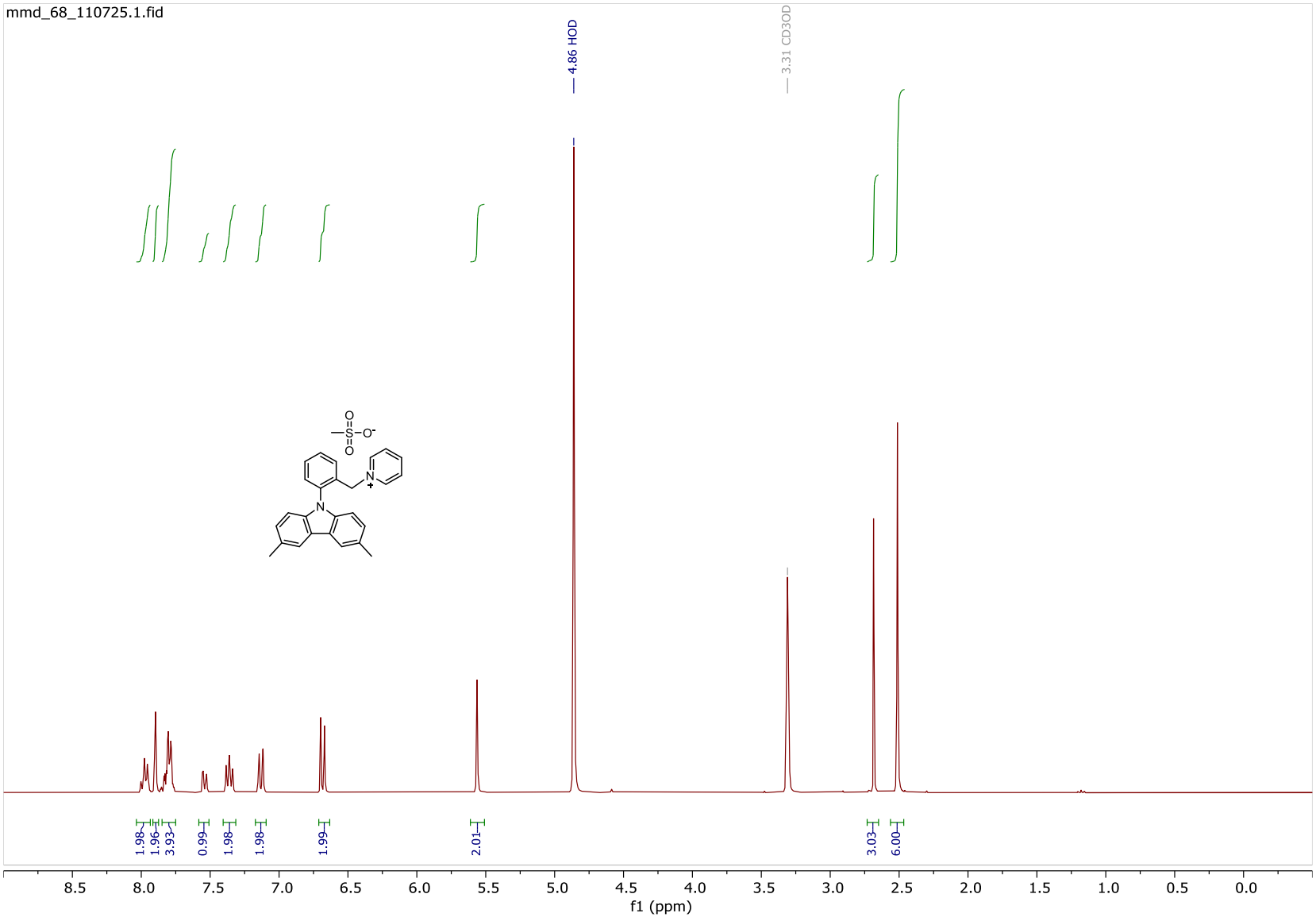

Figure S8. ^{1}H NMR of 1-(2-(3,6-dimethyl-9*H*-carbazol-9-yl)benzyl)pyridin-1-ium methanesulfonate (**5**) **KL1421**

References

(1) Jiao, S.; Tang, W.; Wu, Y.; Li, D.; Tang, Z.; Gao, Z.; Sun, X.; Ma, L.; Cai, H.-L.; Wu, X. S. Photoluminescence Behaviors in Self-Assembly Supramolecular Pyridinium Salts. *Crystal Growth & Design* **2023**, *23* (4), 2106–2119. https://doi.org/10.1021/acs.cgd.2c01054.

(2) Willington, T. D.; Joema, S. E.; Sindhusha, S.; Girisun, T. C. S. Two Photon Absorption Induced Optical Limiting Action of Oxalate Salt of Pyridine for Laser-Assisted Optoelectronic Techniques. *J Mater Sci: Mater Electron* **2021**, *32* (20), 25444–25461. https://doi.org/10.1007/s10854-021-07004-z.

(3) Jesariew, D.; Ilczyszyn, M. M. Crystal Structure, Phase Transition, and Disorder in Pyridinium Methanesulfonate. *Journal of Physics and Chemistry of Solids* **2017**, *104*, 304–314. https://doi.org/10.1016/j.jpcs.2017.01.001.

(4) Srividya, J.; Sivamadhavi, V.; Anbalagan, G. Crystal Structure, Growth, Spectral, Hirshfeld Surface, Optical, Thermal and Third Harmonic Nonlinear Optical Studies of 2-Amino-6-Methyl Pyridine-1-Ium Acetamido Acetate Monohydrate Single Crystal. *J Mater Sci: Mater Electron* **2022**, *33* (35), 26522–26543. https://doi.org/10.1007/s10854-022-09331-1.

(5) Srivastava, A.; Joshi, B. D.; Tandon, P.; Ayala, A. P.; Bansal, A. K.; Grillo, D. Study of Polymorphism in Imatinib Mesylate: A Quantum Chemical Approach Using Electronic and Vibrational Spectra. *Spectrochimica Acta Part A: Molecular and Biomolecular Spectroscopy* **2013**, *103*, 325–332. https://doi.org/10.1016/j.saa.2012.10.066.

(6) Frisch, M. J.; Trucks, G. W.; Schlegel, H. B.; Scuseria, G. E.; Robb, M. A.; Cheeseman, J. R.; Scalmani, G.; Barone, V.; Mennucci, B.; Petersson, G. A.; Nakatsuji, H.; Caricato, M.; Li, X.; Hratchian, H. P.; Izmaylov, A. F.; Bloino, J.; Zheng, G.; Sonnenberg, J. L.; Hada, M.; Ehara, M.; Toyota, K.; Fukuda, R.; Hasegawa, J.; Ishida, M.; Nakajima, T.; Honda, Y.; Kitao, O.; Nakai, H.; Vreven, T.; Jr., J. A. M.; Peralta, J. E.; Ogliaro, F.; Bearpark, M.; Heyd, J. J.; Brothers, E.; Kudin, K. N.; Staroverov, V. N.; Keith, T.; Kobayashi, R.; Normand, J.; Raghavachari, K.; Rendell, A.; Burant, J. C.; Iyengar, S. S.; Tomasi, J.; Cossi, M.; Rega, N.; Millam, J. M.; Klene, M.; Knox, J. E.; Cross, J. B.; Bakken, V.; Adamo, C.; Jaramillo, J.; Gomperts, R.; Stratmann, R. E.; Yazyev, O.; Austin, A. J.; Cammi, R.; Pomelli, C.; Ochterski, J. W.; Martin, R. L.; Morokuma, K.; Zakrzewski, V. G.; Voth, G. A.; Salvador, P.; Dannenberg, J. J.; Dapprich, S.; Daniels, A. D.; Farkas, O.; Foresman, J. B.; Ortiz, J. V.; Cioslowski, J.; Fox, D. J. Gaussian 09, Revision D.01, 2013.

(7) Leduskrasts, K.; Kinens, A.; Suna, E. The Emission Efficiency of Cationic Solid State Luminophores Is Directly Proportional to the Intermolecular Charge Transfer Intensity. *Chem. Commun.* **2023**, *59* (45), 6905. https://doi.org/10.1039/D3CC01674A.